

Revisiting ℓ_1 Loss in Super-Resolution: A Probabilistic View and Beyond

Xiangyu He
NLPR, CASIA

xiangyu.he@nlpr.ia.ac.cn

Jian Cheng
NLPR, CASIA

jcheng@nlpr.ia.ac.cn

Abstract

Super-resolution as an ill-posed problem has many high-resolution candidates for a low-resolution input. However, the popular ℓ_1 loss used to best fit the given HR image fails to consider this fundamental property of non-uniqueness in image restoration. In this work, we fix the missing piece in ℓ_1 loss by formulating super-resolution with neural networks as a probabilistic model. It shows that ℓ_1 loss is equivalent to a degraded likelihood function that removes the randomness from the learning process. By introducing a data-adaptive random variable, we present a new objective function that aims at minimizing the expectation of the reconstruction error over all plausible solutions. The experimental results show consistent improvements on mainstream architectures, with no extra parameter or computing cost at inference time.

1. Introduction

The behavior of single image super-resolution (SISR) networks is primarily driven by the choice of the objective function. Two common examples in SISR are the mean squared error (MSE) loss and the mean absolute error (MAE) loss. Since the long-tested measure peak signal-to-noise ratio (PSNR) is essentially defined on the MSE, pioneer works [11, 20, 21, 38, 41, 66] have largely focused on minimizing the mean squared reconstruction error to achieve high performances.

Due to the ill-posed nature of SISR problem, a low-resolution image \mathbf{x} can be well described as the downsampling result of many high-resolution images $\hat{\mathbf{y}}_{1:k}$. This implies that, in the inverse image reconstruction, the neural network trained by MSE loss, i.e., $\mathbb{E}_{(\mathbf{x}, \hat{\mathbf{y}})} [\sum_i \|f(\mathbf{x}) - \hat{\mathbf{y}}_i\|_2^2]$, will learn to output the *mean* value of all HR targets, i.e., $f(\mathbf{x}) \rightarrow \frac{1}{k} \sum_i \hat{\mathbf{y}}_i$, which best fits the image pairs $\{\mathbf{x}, \hat{\mathbf{y}}_{1:k}\}$ [56]. However, the average of different HR images results in the absence of distinct edges and the blurring effect, which suffers from low image fidelity despite relatively high PSNR. Recently, ℓ_1 loss has received much attention from low-level vision researches, since it is in prac-

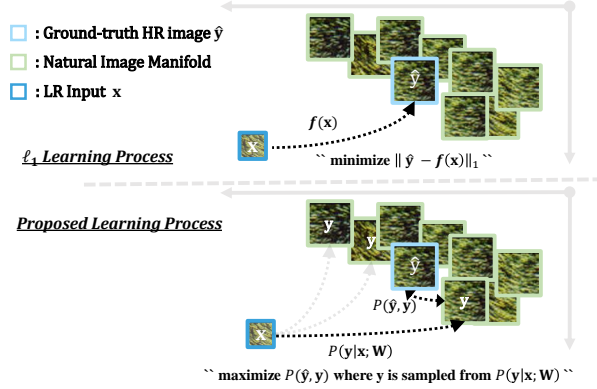


Figure 1. Illustration of the learning process given an LR-HR image pair. ℓ_1 loss only considers the fitting error between model output $f(\mathbf{x})$ and HR image $\hat{\mathbf{y}}$. We propose to learn a one-to-many mapping by introducing $P(\mathbf{y}|\mathbf{x}; \mathbf{W})$ explicitly: 1) first perform a random sampling from $P(\mathbf{y}|\mathbf{x}; \mathbf{W})$ to obtain an underlying natural image \mathbf{y} ; 2) then maximize the likelihood of $\mathbf{y}, \hat{\mathbf{y}}$ co-occurrence. Since we focus on the expected value averaged across all \mathbf{y} instead of any specific sampling result, the learning process serves as a multiple-valued mapping.

ture more robust to the regression-to-the-mean problem in MSE loss [47, 81]. Despite its empirical success in state-of-the-arts super-resolution methods [17, 48, 55, 58, 79, 82], ℓ_1 loss itself has been rarely discussed in the context of image processing.

In probabilistic setting, it is well known that a median is the minimizer of ℓ_1 loss with respect to given targets [63]. In the case of training neural networks over LR-HR image pairs, the situation is quite similar to MSE loss where the network will learn to recover the *median* of all perceptually convincing HR images $\hat{\mathbf{y}}_{1:k}$. However, both ℓ_1 and ℓ_2 loss only capture the median/mean value of the whole solution space, which can be inadequate for estimating any specific solution in high-dimensional predictions, super-resolution in particular.

In this paper, we begin with a simple idea that *it is intuitive to learn a one-to-many mapping since there are plenty of perceptually convincing solutions to an LR input* (Figure 1). Ideally, we may approximate the local manifold, cor-

responding to the ground-truth HR image, by the posterior distribution $P(\mathbf{y}|\mathbf{x}; \mathbf{W})$. Notice that, generative methods are able to capture the more complex distribution of natural images, which inspires us to revisit super-resolution with neural networks from a probabilistic view. In this way, we have the following contributions:

- We derive a loss function for solving SISR by introducing a posterior Gaussian distribution of underlying natural image \mathbf{y} , *i.e.*, $P(\mathbf{y}|\mathbf{x}; \mathbf{W})$, which minimizes the expected reconstruction error across all plausible solutions in \mathbf{y} . The formulated learning process can be easily extended to other $P(\mathbf{y}|\mathbf{x}; \mathbf{W})$ with different distributions such as Laplace.
- The learned standard deviation of $P(\mathbf{y}|\mathbf{x}; \mathbf{W})$ facilitates the HR image regression and, as a by-product, allows us to make meaningful estimates of the model uncertainty in SISR.
- The experimental results show consistent improvements over popular ℓ_1 loss on mainstream networks, without the extra cost at runtime.

2. Related Work

Super-resolution Over the past decades, super-resolution is among the most fundamental low-level vision problems. Early works often formulate the task as an interpolation [3, 44, 45, 78]. Latter studies start to reconstruct high-resolution images in a data-driven way, by estimating the natural image statistics [64, 65] (including deep prior [7, 70]) and exploiting the neighbor embedding [5, 13, 27]. Another group of methods utilizes the self-similarities to learn the inverse mapping [24, 29, 71, 72]. Benefiting from the development of sparse coding, [22, 68, 74] achieve reasonable results on benchmark datasets.

Advances in deep learning have further enhanced the state-of-the-art performance since [20, 21] first introduce a CNN-based SR method. Various CNN architectures have been proposed such as residual networks [37, 38, 47], densely connected networks [69, 80], ode-inspired design [30] and U-Net encoder-decoder networks [16, 49, 50]. In particular, the attention mechanism has become a popular tool for image super-resolution. Both channel attention [79] and non-local technique [17, 58] achieve notable improvements over baseline methods. Recently, self-correlation/self-attention that models the long-distance relationship among similar patches have led to successful results [54, 55, 82], as the large training dataset can be used as a means to capture the global information [14, 46, 73]. Our approach can facilitate the training of deep learning-based methods in a plug-in and play manner.

Loss functions Most learning objects in the literature fall into two main categories: pixel-wise loss and perceptual

loss. The former aims to optimize the full reference metric such as PSNR and SSIM. MSE loss, in particular, is equivalent to PSNR. However, [23, 36, 52] show that ℓ_2 loss results in overly-smooth SR images, and the following works tend to use ℓ_1 during training. In light of the success of knowledge distillation in image recognition, [26, 42] use loss functions in the feature space to enhance the performance of student networks. Our work also falls into this category. We propose to learn from a posterior distribution instead of best-fitting ground-truth images.

Perceptual loss tackles the problem by employing generative adversarial networks [18, 52], especially in super-resolution with large upscaling factors (*e.g.*, 4 \times , 8 \times) [41, 75]. The ImageNet pre-trained networks are commonly used as a discriminator loss [7, 23, 36], which leads to high-frequency details and perceptually satisfying results in the sense. Our approach can be compatible with those adversarial settings as the content loss term in a perceptual loss.

The most related work is Noise2noise [43], which suffers from inaccurate gradient directions (details in Section 3.3). We solve this problem by a well-bounded gradient step and point out that [43] indeed serves as a special case of our approach. Noise2Self [4] assumes that noise in each patch is independent of other patches, which can not hold responsible when it comes to the content of images instead of noise. Self2Self [60] presents dropout in both image and feature space to reduce prediction variances, which is also compatible with our loss functions.

Model uncertainty Despite their unprecedented power to solve the inverse problem, deep learning-based SR methods are prone to make mistakes. As deep models are widely used in computer-aided diagnosis [15, 76], it is crucial to better understand the confidence of neural networks in their predictions. That is, the SR network may provide uncertainty about the generated super-resolved images: which part is “real” and when we should be cautious.

[28] first develops a framework for modeling uncertainty, which is hard to describe the modern deep neural networks. Recently, Monte Carlo Dropout [25] presents a practical solution to estimate uncertainty via the dropout layer. [67] further shows that networks trained with Batch-Normalization [35] (BN) is an approximate Bayesian model and allows an uncertainty estimation by sampling the network’s BN parameters. Unfortunately, neither of them was used in recent SR networks, which disables the variational inference in those approximate Bayesian models. Instead, we model the posterior distribution $P(\mathbf{y}|\mathbf{x}; \mathbf{W})$ explicitly, as a by-product, the estimated standard deviation facilitates the uncertainty estimation for SISR.

3. Analysis

3.1. Probabilistic Modeling

From a statistical viewpoint, we are interested in the point estimation of the model parameters \mathbf{W} , used in the following likelihood function:

$$\max_{\mathbf{W}} \mathcal{L}(\mathbf{W}|\hat{\mathbf{y}}) = P(\hat{\mathbf{y}}|\mathbf{x}; \mathbf{W}) \quad (1)$$

where \mathbf{W} , $\hat{\mathbf{y}}$ and \mathbf{x} indicate weights, observed ground-truth labels and inputs respectively. Super-resolution using convolutional neural networks also fall into this form, that learning parameters \mathbf{W} w.r.t. an inference function $f(\mathbf{x})$ from LR-HR image pairs directly.

In contrast to finding a one-to-one mapping between corrupted images and targets implied by $f(\mathbf{x})$, we begin with a subtle point: in reality, the mapping from $\hat{\mathbf{y}}$ to \mathbf{x} is surjective. For example, a single LR image \mathbf{x} may correspond to the downsampling result of multiple natural images. Hence, *it is intuitive to recover or approximate the local image manifold instead of simply fitting the high-resolution image $\hat{\mathbf{y}}$.*

Objective function The idea is to explicitly estimate a posterior distribution $P(\mathbf{y}|\mathbf{x}; \mathbf{W})$ where \mathbf{y} refers to (multiple) underlying natural images with the size of $H \times W$. Then, the observed HR image $\hat{\mathbf{y}}$ should look like its counterpart \mathbf{y} sampled from $P(\mathbf{y}|\mathbf{x}; \mathbf{W})$, with high probability. Formally, our goal is to maximize the following conditional joint density function:

$$P(\hat{\mathbf{y}}, \mathbf{y}|\mathbf{x}; \mathbf{W}) = P(\hat{\mathbf{y}}|\mathbf{y})P(\mathbf{y}|\mathbf{x}; \mathbf{W}) \quad (2)$$

where $P(\hat{\mathbf{y}}|\mathbf{y})$ is a measure of the probability that $\hat{\mathbf{y}}$ being observed given \mathbf{y} . Note that, there are plenty of \mathbf{y} can serve as the perceptually convincing solution to Eq.(2) then, as is common in machine learning, we take the expectation of that formula to be optimized:

$$\mathbb{E}_{\mathbf{y} \sim P(\mathbf{y}|\mathbf{x}; \mathbf{W})} [P(\hat{\mathbf{y}}|\mathbf{y})]. \quad (3)$$

To solve Eq.(3), we will first need to deal with $P(\mathbf{y}|\mathbf{x}; \mathbf{W})$, the distribution of underlying natural images \mathbf{y} consistent with the low-resolution \mathbf{x} .

Optimizing the objective Based on the finding of *non-local means* [8, 9] that each pixel is obtained as a weighted average of pixels centered at regions similar to the reference and the central limit theorem (CLT), we shall model $P(\mathbf{y}|\mathbf{x}; \mathbf{W})$ as a multivariate normal distribution¹:

$$P(\mathbf{y}|\mathbf{x}; \mathbf{W}) \sim \mathcal{N}(\boldsymbol{\mu}_{(\mathbf{x}; \mathbf{W})}; \boldsymbol{\Sigma}_{(\mathbf{x}; \mathbf{W})}) \quad (4)$$

where mean $\boldsymbol{\mu}$ and covariance $\boldsymbol{\Sigma}$ are outputs of multi-layer neural networks with parameters \mathbf{W} . $\boldsymbol{\sigma}^2$ corresponds to the

¹The distribution of $P_{\mathbf{y}|\mathbf{x}}$ is not required to be Gaussian: for instance, if \mathbf{y} is in practice more-Laplace, then $P_{\mathbf{y}|\mathbf{x}}$ might be re-parameterized as $\boldsymbol{\mu} - \boldsymbol{\sigma} * \text{sgn}(\mathbf{z}) * \ln(1 - 2|\mathbf{z}|)$, $\mathbf{z} \sim \mathcal{N}(\mathbf{0}, \mathbf{1})$.

diagonal elements in $\boldsymbol{\Sigma}$. However, the expectation in Eq.(3) still involves sampling \mathbf{y} from $P(\mathbf{y}|\mathbf{x}; \mathbf{W})$ which is a non-differentiable operation. To allow the backprop through \mathbf{y} , we use one of the most common trick in machine learning, the “reparameterization” [40], to move the sampling to the random variable $\mathbf{z} \sim \mathcal{N}(\mathbf{0}, \mathbf{1})$:

$$\mathbb{E}_{\mathbf{y} \sim P(\mathbf{y}|\mathbf{x}; \mathbf{W})} [P(\hat{\mathbf{y}}|\mathbf{y})] = \mathbb{E}_{\mathbf{z} \sim \mathcal{N}(\mathbf{0}, \mathbf{1})} [P(\hat{\mathbf{y}}|\boldsymbol{\mu} + \boldsymbol{\sigma} * \mathbf{z})]$$

where \mathbf{y} is reformulated as $\boldsymbol{\mu} + \boldsymbol{\sigma} * \mathbf{z}$ and “*” indicates elementwise product. Then, we can conduct the standard gradient descent and the gradient averaged over \mathbf{z} should converge to the actual gradient of Eq.(3).

Similarly, as [7], we consider the conditional model defined by the Gibbs distribution (also known as Boltzmann distribution):

$$P(\hat{\mathbf{y}}|\mathbf{y}) \propto \prod_i^{H \times W} \exp\left(-\frac{|\hat{\mathbf{y}}_i - \mathbf{y}_i|}{kT}\right) \quad (5)$$

where the corresponding Gibbs energy is in the form of $\|\hat{\mathbf{y}} - \mathbf{y}\|_1$ and kT is the fixed partition function. The model (5) assumes that \mathbf{y} , looks like the observed ground-truth image $\hat{\mathbf{y}}$, is likely to be a strong evidence for $\hat{\mathbf{y}}$ occurring. We can now get both $P(\mathbf{y}|\mathbf{x}; \mathbf{W})$ and $P(\hat{\mathbf{y}}|\mathbf{y})$ into Eq.(3) then apply negative log-likelihood to the final objective for computational convenience:

$$\min \mathbb{E}_{\mathbf{z}} \left[\frac{1}{kT} \sum_i^{H \times W} |\hat{\mathbf{y}}_i - (\boldsymbol{\mu}_i + \boldsymbol{\sigma}_i * \mathbf{z})| \right]. \quad (6)$$

This equation implies a two-branch network ($\boldsymbol{\mu}$ and $\boldsymbol{\sigma}$) that requires randomness during training. The expectation on the data-independent random variable \mathbf{z} allows us to move the gradient symbol into the expectation to finish the standard stochastic gradient descent [19]. For notational simplicity, we shall in the remaining text denote Eq.(6) as $\mathbb{E}_{\mathbf{z}} [\|\hat{\mathbf{y}} - (\boldsymbol{\mu} + \boldsymbol{\sigma} * \mathbf{z})\|_1]$.

3.2. Revisiting ℓ_1 Loss

According to Jensen’s inequality, for any measurable convex function $f(\cdot)$, we have $\mathbb{E}[f(\mathbf{z})] \geq f(\mathbb{E}[\mathbf{z}])$. Since every p -norm is convex and $\mathbf{z} \sim \mathcal{N}(\mathbf{0}, \mathbf{1})$, then we have

$$\begin{aligned} \mathbb{E}_{\mathbf{z}} [\|\hat{\mathbf{y}} - (\boldsymbol{\mu} + \boldsymbol{\sigma} * \mathbf{z})\|_1] &\geq \|\hat{\mathbf{y}} - (\boldsymbol{\mu} + \boldsymbol{\sigma} * \mathbb{E}_{\mathbf{z}}[\mathbf{z}])\|_1 \\ &= \|\hat{\mathbf{y}} - \boldsymbol{\mu}\|_1. \end{aligned}$$

Notice that the proposed learning target (6) actually serves as an upper bound of the popular ℓ_1 loss function. In other words, ℓ_1 loss also suffers from the degradation that loses the randomness during training and is confined to the given HR images $\hat{\mathbf{y}}$. Though the optimal solution for the original function and for the upper bound are indeed different,

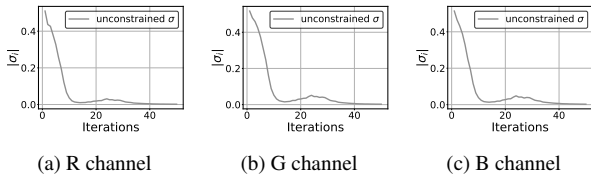


Figure 2. The degradation curves of σ_i during training. When σ_i approaching zero, Eq.(6) is equivalent to ℓ_1 loss.

the probabilistic learning object can relax the deterministic learning process at each step by focusing on the expectation of the loss function.

Owing to the reparameterization trick [40], learning probabilistic model via Eq.(6) seems straightforward. However, there exists a trivial solution to easily bridge the Jensen gap (i.e., $\mathbb{E}[f(\mathbf{z})] = f(\mathbb{E}[\mathbf{z}])$) such that $\sigma \in \vec{0}$. As shown in Figure 2, the output of σ branch gradually approaches zero which ultimately eliminates the randomness in our learning target. Similar degradation also occurs in Variational Auto-Encoder (VAE). In a nutshell, a VAE is an auto-encoder when latent variable \mathbf{z} that determines encodings distribution lose randomness². In light of this, we focus on avoiding the degradation of σ in the following section.

3.3. Beyond ℓ_1 Loss

Data-independent σ The simplest way is to remove the trainable σ branch and let σ_i be a small constant k invisible to the human eye. Then, $P(\mathbf{y}|\mathbf{x}; \mathbf{W}) \sim \mathcal{N}(\boldsymbol{\mu}; k^2 \mathbf{I})$ where \mathbf{I} refers to an identity matrix. Contracting this term into Eq.(6) and rearranging yields:

$$\mathbb{E}_{\mathbf{z}} \left[\|\hat{\mathbf{y}} - (\boldsymbol{\mu} + k \cdot \mathbf{z})\|_1 \right] = \mathbb{E}_{\mathbf{z}} \left[\underbrace{\|(\hat{\mathbf{y}} + \mathbf{z}') - \boldsymbol{\mu}\|_1}_{\text{Noised HR}} \right] \quad (7)$$

where \mathbf{z}' is an additive Gaussian noise $\mathcal{N}(0, k)$ and $k \neq 0$. The left hand side of this equation is something we hope to optimize via backward propagation. The right hand side serves is the core of Noise2Noise [43] that restores corrupted images without clean data, i.e., learning super-resolution by only looking at noised HR images.

Though the performance of training on corrupted observations may approach its clean counterpart [43], the noise term can do harm to the optimization process. To be specific, we expect $\boldsymbol{\mu}$ to approach $\hat{\mathbf{y}}$ via stochastic gradient descent. However, for some \mathbf{z}' satisfying $((\hat{\mathbf{y}}_i - \boldsymbol{\mu}_i) + \mathbf{z}')(\hat{\mathbf{y}}_i -$

²VAE regularises its random latent variable \mathbf{z} towards Normal distribution that enables generative process [19]. Otherwise, the latent space will converge to a single point instead of a distribution. That is, VAE degrades into an one-to-one mapping given input images, i.e., an (deterministic) auto-encoder.

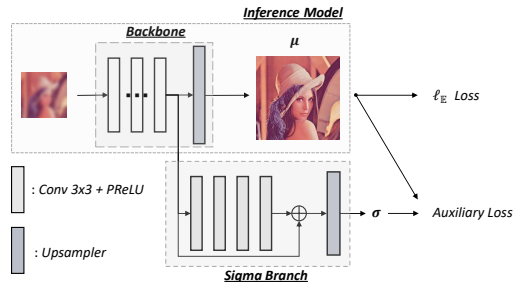


Figure 3. An illustration of the proposed learning scheme and the sigma branch. The newly added branch includes two operations: four Conv+PReLU blocks serve as a mapping function and the upsampler (Pixelshuffle coupled with 3×3 convolution) adjusts the output size. “ $\ell_{\mathbb{E}}$ ” and “Auxiliary Loss” correspond to Eq.(8) and Eq.(10) respectively. We use $\boldsymbol{\mu}$ as the super-resolved image at inference time.

$\boldsymbol{\mu}_i) < 0$, we have

$$\text{sgn}\left(\frac{\partial \|\hat{\mathbf{y}} + \mathbf{z}' - \boldsymbol{\mu}\|_1}{\partial \boldsymbol{\mu}_i}\right) = -1 \cdot \text{sgn}\left(\frac{\partial \|\hat{\mathbf{y}} - \boldsymbol{\mu}\|_1}{\partial \boldsymbol{\mu}_i}\right)$$

where \mathbf{z}' results in gradient ascent instead of descent, which ultimately hinders $\boldsymbol{\mu}$ from fitting $\hat{\mathbf{y}}$. To get a good estimate of the proper gradient, it would require sampling massive noised observations given a single clean image, which would be expensive. Hence, we hope to find some σ that run correct backprop efficiently and retain randomness.

Data-adaptive σ Fortunately, a delicate σ gives a definite answer to both. The full equation we want to optimize is:

$$\min_{\boldsymbol{\mu}} \mathbb{E}_{\mathbf{z}} \left[\|\hat{\mathbf{y}} - (\boldsymbol{\mu} + |\hat{\mathbf{y}} - \boldsymbol{\mu}| * \mathbf{z})\|_1 \right] \quad (8)$$

where $|\hat{\mathbf{y}} - \boldsymbol{\mu}|$ corresponds to the σ term and $|\cdot|$ refers to element-wise absolute function. We shall denote Eq.(8) as $\ell_{\mathbb{E}}$ in the remaining text for simplicity.

From the view of Eq.(7), $\ell_{\mathbb{E}}$ is also in the form of adding some (data-adaptive) noise to HR images. However, for Eq.(8), we allow the backprop through $|\hat{\mathbf{y}} - \boldsymbol{\mu}|$ instead of regarding it as a scaling factor, which contributes to the following property: For any $\mathbf{z} \sim \mathcal{N}(0, 1)$, we have

$$\text{sgn}\left(\frac{\partial \ell_{\mathbb{E}}}{\partial \boldsymbol{\mu}_i}\right) = \text{sgn}\left(\frac{\partial \|\hat{\mathbf{y}} - \boldsymbol{\mu}\|_1}{\partial \boldsymbol{\mu}_i}\right), \quad \left| \mathbb{E}_{\mathbf{z}} \left[\frac{\partial \ell_{\mathbb{E}}}{\partial \boldsymbol{\mu}_i} \right] \right| \approx 1. \quad (9)$$

Note that the gradient direction is always making $\boldsymbol{\mu}$ approach $\hat{\mathbf{y}}$ and the step-size converges to nearly one. Therefore, we can safely average the gradient of $\nabla_{\mathbf{W}} \ell_{\mathbb{E}}$ over arbitrarily many samplings of \mathbf{z} and training images \mathbf{x} , without the risk of gradient ascent or the problem of vanishing/exploding gradient. Due to the ill-posed nature of super-resolution, $|\hat{\mathbf{y}} - \boldsymbol{\mu}|$ can never be a zero vector then the randomness of (8) will be preserved.

It is shown that $|\hat{\mathbf{y}} - \boldsymbol{\mu}|$ plays a core role in learning $\boldsymbol{\mu}$ and serves as σ in $\ell_{\mathbb{E}}$ loss, which inspires us to re-fetch the σ

branch to perform the following multi-task learning except $\ell_{\mathbb{E}}$ loss:

$$\min_{\sigma} \beta \cdot \|\hat{y} - \mu - \sigma\|_1 \quad (10)$$

where β is a penalty factor and μ is detached from backward propagation. This equation also, as a by-product, allows us to make a rough estimate of the model uncertainty in SISR via the prediction of σ , *e.g.*, small σ_i means we can be certain of the super-resolved image produced by neural networks, otherwise should be less confident (details in Section 4.6). Finally, Figure 3 further illustrates the overall structure of the proposed scheme.

4. Experiments

4.1. Dataset

For Bicubic image SR, following the common setting in [2, 17, 30, 47, 58, 82], we conduct all experiments on the 1st-800th images from DIV2K [1] training set then evaluate our models on five benchmarks: Set5 [6], Set14 [77], B100 [51], Urban100 [32] and Manga109 [53] with scale factors 2 \times , 3 \times , 4 \times . To make a fair comparison with early works trained on the tiny dataset [68], we also cite the reproduced DIV2K results [42] in Table 4. For real-world SR, we use the same dataset and training settings proposed in RealSR benchmark [12]. We report PSNR and SSIM on the Y channel in YCbCr space and ignore the same amount of pixels as scales from the border.

4.2. Training Details

We use low-resolution RGB image patches with the size of 48 \times 48 for training. All HR-LR image pairs are randomly rotated by 90 $^{\circ}$, 180 $^{\circ}$, 270 $^{\circ}$ and flipped horizontally [47]. We set the mini-batch size to 16. Our models are trained by Adam optimizer [39] with $\beta_1 = 0.9$, $\beta_2 = 0.999$, and $\epsilon = 10^{-8}$. The initial learning rate is set to 10^{-4} and decreases to half at every 2×10^5 mini-batch updates. The total training cost is 10^6 iterations [47]. For RealSR, as described in [12], the training patch size is 192 \times 192 and learning rate is fixed at 10^{-4} . Other details are the same as classical SR. We use the PyTorch framework [59] to implement our methods with an NVIDIA Tesla V100 GPU.

4.3. Ablation Studies

We first present an ablation analysis on each object function in our learning process and report quantitative results in terms of average PSNR and SSIM on Set14 [77] with the scale factor of 2. The baseline results in Table 1 (*i.e.*, first row) are obtained using EDSR pre-trained model³. In the case of training neural networks by Eq.(10) (*i.e.*, third

³https://cv.snu.ac.kr/research/EDSR/models/edsr_baseline_x2-1bc95232.pt

Table 1. EDSR-baseline [47] results on Set14 (2 \times) for different learning targets. We use the best setting in the following experiments.

ℓ_1	Eq.(8)	Eq.(10)	PSNR (dB)	SSIM	Training cost
✓			33.57	0.9175	2.00 ms/iter
	✓		33.68	0.9181	2.06 ms/iter
		✓	33.57	0.9176	2.16 ms/iter
✓		✓	33.64	0.9180	2.71 ms/iter
	✓	✓	33.71	0.9185	2.77 ms/iter

Table 2. Ablation study on the penalty factor β . (EDSR-baseline [47] on Set14 2 \times)

β	0.001	0.005	0.01	0.05	0.1
PSNR (dB)	33.605	33.641	33.707	33.663	33.647
SSIM	0.9176	0.9181	0.9185	0.9184	0.9178

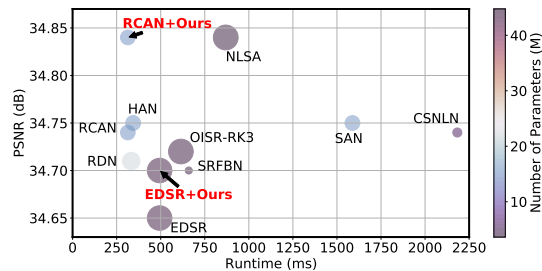


Figure 4. Trade-off between the model size and the average PSNR on Set5 [6] (3 \times). The marker size indicates the number of parameters. The running time is measured on an 720P SR image. (Best viewed in color.)

row), we run the backpropagation through both μ and σ to allow the prediction of super-resolved images via μ branch. The following rows illustrate that both $\ell_{\mathbb{E}}$ loss (Eq.(8)) and the multi-task learning (Eq.(10)) contribute to higher performances than ℓ_1 baseline. When applying both settings to the original network, we can further improve the PSNR and SSIM results. In the following experiments, we use “Eq.(8)+Eq.(10)” as the learning target.

Table 2 indicates that a proper β matters in the balance between reconstruction loss $\ell_{\mathbb{E}}$ and the auxiliary term. Fortunately, 0.01 seems to perform well in most cases. For simplicity, we set the channel number of the sigma branch to 160 and introduce a sigmoid function to normalize its output. In our experiments, we notice that nearly half of the estimated σ approach zero, which correspond to the low-frequency/smooth parts of the high-resolution images (as shown in Figure 7). In light of this, we set $|\hat{y}_i - \mu_i|$ that is less than the average to zero and focus on the hard samples. Due to the limited computing resource, we did not conduct an ablation study on the structure of the sigma branch, instead simply borrowing the idea of Conv+PReLU proposed in [21], shown in Figure 3.

Table 3. Quantitative comparison with lightweight models. Our approach improves the performance of early baseline methods to the state-of-the-art. It is shown that networks with simple structures such as EDSR [47] can be competitive with recent elaborate-designed networks. When coupled with efficient models (e.g., CARN [2], IDN [34]), the improvement is consistent as shown in Table 4.

Scale	Methods	#Param.	MAC	Runtime	Set5 [6]		Set14 [77]		B100 [51]		Urban100 [32]	
					PSNR	SSIM	PSNR	SSIM	PSNR	SSIM	PSNR	SSIM
2×	VDSR [37]	668K	614.7G	120.8ms	37.53	0.9587	33.03	0.9124	31.90	0.8960	30.76	0.9140
	VDSR+Ours				37.83	0.9600	33.40	0.9158	32.05	0.8983	31.59	0.9226
	EDSR-baseline [47]	1370K	316.2G	56.5ms	37.99	0.9604	33.57	0.9175	32.16	0.8994	31.98	0.9272
	EDSR-baseline+Ours				38.02	0.9606	33.71	0.9185	32.18	0.9001	32.19	0.9292
	CARN [2]				964K	223.4G	56.7ms	37.76	0.9590	33.52	0.9166	32.09
	IMDN [33]	694K	159.6G	43.2ms	38.00	0.9605	33.63	0.9177	32.19	0.8996	32.17	0.9283
OISR [30]	1372K	316.2G	68.8ms	38.02	0.9605	33.62	0.9178	32.20	0.9000	32.21	0.9290	
3×	VDSR [37]	668K	614.7G	117.3ms	33.66	0.9213	29.77	0.8314	28.82	0.7976	27.14	0.8279
	VDSR+Ours				34.18	0.9249	30.18	0.8395	28.99	0.8028	27.80	0.8436
	EDSR-baseline [47]	1555K	160.1G	30.4ms	34.37	0.9270	30.28	0.8417	29.09	0.8052	28.15	0.8527
	EDSR-baseline+Ours				34.41	0.9271	30.38	0.8435	29.12	0.8062	28.22	0.8543
	CARN [2]				1149K	118.9G	30.7ms	34.29	0.9255	30.29	0.8407	29.06
	IMDN [33]	703K	71.7G	22.4ms	34.36	0.9270	30.32	0.8417	29.09	0.8046	28.17	0.8519
OISR [30]	1557K	160.1G	36.2ms	34.39	0.9272	30.35	0.8426	29.11	0.8058	28.24	0.8544	
4×	VDSR [37]	668K	614.7G	121.4ms	31.35	0.8838	28.01	0.7674	27.29	0.7251	25.18	0.7524
	VDSR+Ours				31.89	0.8900	28.45	0.7778	27.46	0.7327	25.76	0.7734
	EDSR-baseline [47]	1518K	114.2G	21.6ms	32.09	0.8938	28.58	0.7813	27.57	0.7357	26.04	0.7849
	EDSR-baseline+Ours				32.15	0.8933	28.65	0.7831	27.59	0.7377	26.15	0.7885
	CARN [2]				1112K	91.1G	22.5ms	32.13	0.8937	28.60	0.7806	27.58
	IMDN [33]	715K	41.1G	11.6ms	32.21	0.8948	28.58	0.7811	27.56	0.7353	26.04	0.7838
OISR [30]	1520K	114.2G	24.9ms	32.14	0.8947	28.63	0.7819	27.60	0.7369	26.17	0.7888	

Table 4. PSNR comparison with recently proposed loss functions for SISR. PISR [42] is a Knowledge Distillation framework where a “Teacher” network is required during training. “DIV2K” means models reproduced by [42] using DIV2K dataset with ℓ_1 loss. “EDSR-baseline” refers to the baseline model in [47].

Model	Loss Type	2×	3×	4×
		Set5/B100	Set5/B100	Set5/B100
VDSR	ℓ_2	37.53 / 31.90	33.67 / 28.82	31.35 / 27.29
	DIV2K [1]	37.64 / 31.96	33.80 / 28.83	31.37 / 27.25
	Edge [61]	37.70 / 31.98	33.82 / 28.88	31.45 / 27.35
	Riemann [57]	37.72 / 32.04	33.83 / 28.99	31.58 / 27.41
	Teacher [42]	37.77 / 32.00	33.85 / 28.86	31.51 / 27.29
	Ours	37.83 / 32.05	34.18 / 28.99	31.89 / 27.46
IDN	ℓ_1	37.83 / 32.08	34.11 / 28.95	31.82 / 27.41
	DIV2K [1]	37.88 / 32.12	34.22 / 29.02	32.03 / 27.49
	Teacher [42]	37.93 / 32.14	34.31 / 29.03	32.01 / 27.51
	Ours	37.91 / 32.11	34.33 / 29.04	32.09 / 27.53
CARN	ℓ_1	37.76 / 32.09	34.29 / 29.06	32.13 / 27.58
	Teacher [42]	37.82 / 32.08	34.10 / 28.95	31.83 / 27.45
	Ours	37.95 / 32.13	34.37 / 29.08	32.18 / 27.59
EDSR-baseline	ℓ_1	37.99 / 32.16	34.37 / 29.09	32.09 / 27.57
	Riemann [57]	37.87 / 32.14	34.40 / 29.05	32.15 / 27.56
	Ours	38.02 / 32.20	34.43 / 29.11	32.15 / 27.59

4.4. Quantitative Results

Figure 4 shows the performance comparison of our approach coupled with various SR methods to state-of-the-arts in terms of the number of operations and parameters. We notably improve the Pareto frontier with no extra parameter or computing cost at inference time. When compared with recent learning strategies for image restoration, ours performs the best at most cases (Table 4), even surpasses the knowledge distillation method PISR [42]. Listed SR meth-

Table 5. Average PSNR (dB) for different models on RealSR testing set. We directly cite SRResNet and RCAN results reported in RealSR benchmark [12]. RCAN used in [12] is smaller than the original model. The running time is measured on a 1200 × 2200 SR image.

Model	#Param.	Runtime	PSNR(dB)		
			2×	3×	4×
Bicubic	–	–	32.61	29.34	27.99
DPS [12]	1.26M	122.8ms	32.71	32.20	28.69
KPN [12]	1.48M	274.8ms	33.86	30.39	28.90
LP-KPN [12]	1.43M	181.3ms	33.90	30.42	28.92
SRResNet [41]	1.31M	143.1ms	33.69	30.18	28.67
SRResNet+Ours			33.87	30.49	28.84
RCAN [79]	8.18M	510.6ms	33.87	30.40	28.88
RCAN+Ours			34.06	30.63	29.00

ods generally benefit from the proposed scheme except for IDN [34] with the scale factor of 2 on B100 [51].

We further detail the performance of our approach in contrast to recent lightweight networks [2, 30, 33] in Table 3. To well describe different methods, we report the number of parameters, operations required to reconstruct a 720P image, and its average runtime speed measured on an NVIDIA Titan RTX GPU. From Table 3, we observe that VDSR [37] trained by the proposed learning process outperforms baselines by a large margin, consistently for all scaling factors. Former state-of-the-art EDSR-baseline [47] with our approach also shows competitive results with recent well-designed lightweight SR methods. We further conduct experiments on the large BI degradation model EDSR [47]. As shown in Table 6, the original model has

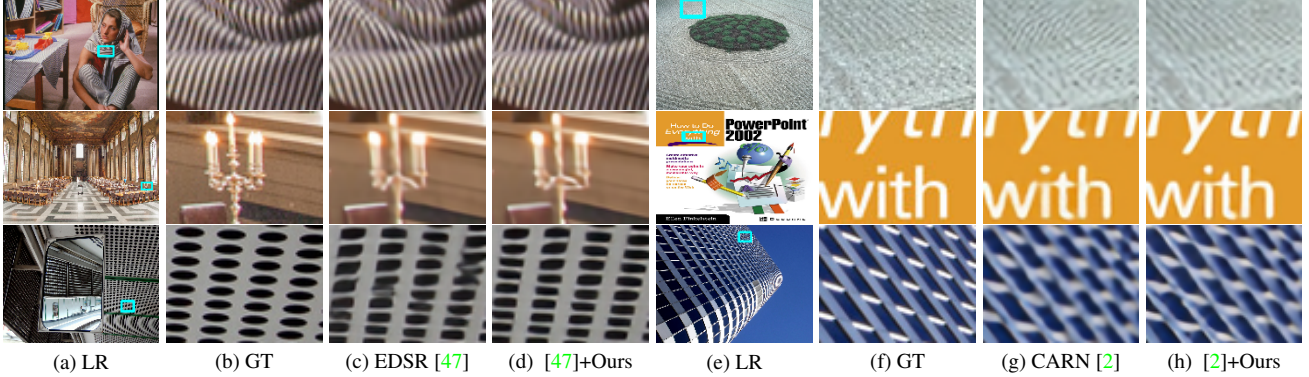


Figure 5. Visual comparison for 2 \times , 3 \times and 4 \times SR with BI models on benchmark datasets.

Table 6. Quantitative comparison with computing-intensive models. We report the multiply-accumulate operations (MAC) and real runtime cost, required to reconstruct a 1280 \times 720 HR image. RCAN [79] coupled with our methods can be competitive with recent leading works.

Scale	Methods	#Param.	Runtime	Set5 [6]		Set14 [77]		B100 [51]		Urban100 [32]		Manga109 [53]	
				PSNR	SSIM	PSNR	SSIM	PSNR	SSIM	PSNR	SSIM	PSNR	SSIM
2 \times	EDSR [47]	40.73M	1003.6ms	38.11	0.9602	33.92	0.9195	32.32	0.9013	32.93	0.9351	39.10	0.9773
	EDSR+Ours			38.24	0.9613	34.05	0.9209	32.36	0.9020	32.96	0.9360	39.19	0.9780
	RCAN [79]	15.44M	667.8ms	38.27	0.9614	34.12	0.9216	32.41	0.9027	33.34	0.9384	39.44	0.9786
	RCAN+Ours			38.25	0.9615	34.16	0.9231	32.40	0.9025	33.19	0.9381	39.41	0.9785
	SAN [17]	15.71M	4817.6ms	38.31	0.9620	34.07	0.9213	32.42	0.9028	33.10	0.9370	39.32	0.9792
	HAN [58]	15.92M	743.3ms	38.27	0.9614	34.16	0.9217	32.41	0.9027	33.35	0.9385	39.46	0.9785
NLSA [54]	41.80M	1915.8ms	38.34	0.9618	34.08	0.9231	32.43	0.9027	33.42	0.9394	39.59	0.9789	
3 \times	EDSR [47]	43.68M	493.8ms	34.65	0.9280	30.52	0.8462	29.25	0.8093	28.80	0.8653	34.17	0.9476
	EDSR+Ours			34.70	0.9295	30.58	0.8467	29.28	0.8100	28.87	0.8669	34.18	0.9487
	RCAN [79]	15.63M	313.4ms	34.74	0.9299	30.65	0.8482	29.32	0.8111	29.09	0.8702	34.44	0.9499
	RCAN+Ours			34.84	0.9304	30.70	0.8493	29.33	0.8112	29.14	0.8716	34.56	0.9504
	SAN [17]	15.90M	1,587.9ms	34.75	0.9300	30.59	0.8476	29.33	0.8112	28.93	0.8671	34.30	0.9494
	HAN [58]	16.11M	343.7ms	34.75	0.9299	30.67	0.8483	29.32	0.8110	29.10	0.8705	34.48	0.9500
NLSA [54]	44.75M	869.0ms	34.84	0.9306	30.70	0.8485	29.34	0.8117	29.25	0.8726	34.57	0.9508	
4 \times	EDSR [47]	43.10M	322.6ms	32.46	0.8968	28.80	0.7876	27.71	0.7420	26.64	0.8033	31.02	0.9148
	EDSR+Ours			32.48	0.8985	28.86	0.7883	27.74	0.7423	26.68	0.8045	31.12	0.9165
	RCAN [79]	15.59M	181.1ms	32.63	0.9002	28.87	0.7889	27.77	0.7436	26.82	0.8087	31.22	0.9173
	RCAN+Ours			32.69	0.9005	28.89	0.7892	27.78	0.7437	26.87	0.8094	31.40	0.9185
	SAN [17]	15.86M	880.0ms	32.64	0.9003	28.92	0.7888	27.78	0.7436	26.79	0.8068	31.18	0.9169
	HAN [58]	16.07M	196.8ms	32.64	0.9002	28.90	0.7890	27.80	0.7442	26.85	0.8094	31.42	0.9177
NLSA [54]	44.15M	523.6ms	32.59	0.9000	28.87	0.7891	27.78	0.7444	26.96	0.8109	31.27	0.9184	

achieved high PSNR/SSIM on each dataset, while ours can further enhance the performance in most cases.

4.5. Qualitative Results

To further illustrate the analysis above, we show visual comparisons in Figure 5 and 6. Bicubic downsampling results in the loss of texture details and structure information, which induces super-resolved images with blurring and artifacts. Even worse, EDSR generates perceptually convincing results such as “barbara” in Set14 (first row in Figure 5c). However, the SR image contains several lines with wrong directions. Instead, our models can recover them being more faithful to the ground truth. CARN [2] with ours also obtains much better results by recovering more informative details.

Despite the promising results, networks can make mistakes when exposed to unseen data outside the trained dis-

tribution. In this case, we expect information about model uncertainty in addition to the SR images.

4.6. Model Uncertainty

By introducing a posterior distribution $P(\mathbf{y}|\mathbf{x}; \mathbf{W})$, we can easily use the predicted σ as the estimated model uncertainty (Figure 7e). Following previous Bayesian models [10, 25, 31, 67], we evaluate uncertainty quality based on the standard metric Predictive Log Likelihood (PLL):

$$\text{PLL}(f(\mathbf{x}), (\hat{\mathbf{y}}, \mathbf{x})) = \log P(\hat{\mathbf{y}}|f(\mathbf{x})) \quad (11)$$

where $P(\hat{\mathbf{y}}|f(\mathbf{x}))$ is the probability of target $\hat{\mathbf{y}}$ generated by a probabilistic model $f(\mathbf{x})$. In this paper, $f(\mathbf{x})$ corresponds to the multivariate Gaussian $\mathcal{N}(\boldsymbol{\mu}, \boldsymbol{\sigma}^2)$ with predicted mean $\boldsymbol{\mu}$ and standard deviation $\boldsymbol{\sigma}$. $P(\hat{\mathbf{y}}|f(\mathbf{x}))$ is the Gaussian probability density function (PDF) evaluated at $\hat{\mathbf{y}}$.

We report the average PLL of our approach coupled

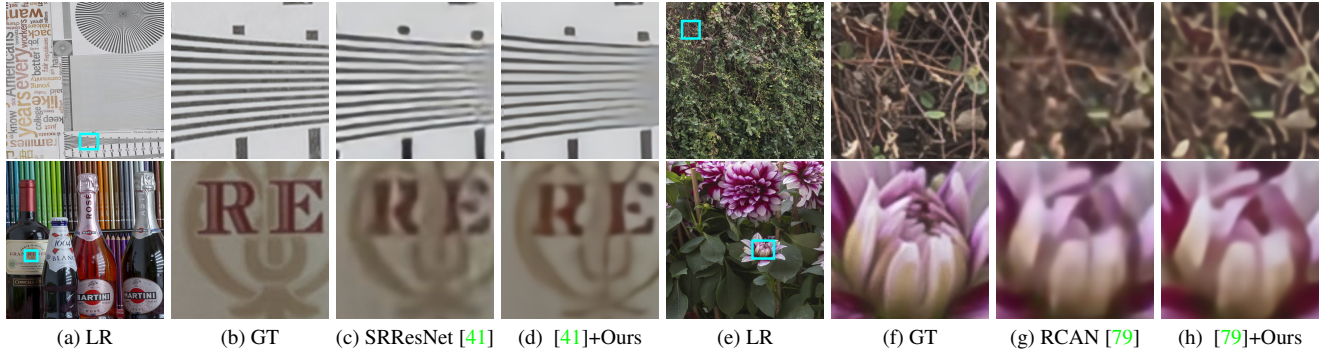


Figure 6. SR results on 3 \times and 4 \times RealSR testing set by different methods.

Table 7. The quality of model uncertainty measured on test datasets. PLL (higher is better \uparrow) is the widely accepted uncertainty metric. Since uncertainty should reflect underlying mistakes in super-resolved images, PSNR (\uparrow) between the predicted uncertainty σ and the actual fitting error $|\hat{y} - \mu|$ is also reported (*i.e.*, PSNR between Fig. 7e and Fig. 7d).

Model	Scale	S5 [6]	S14 [77]	B100 [51]	U100 [32]
		PLL/PSNR	PLL/PSNR	PLL/PSNR	PLL/PSNR
EDSR	2 \times	2.60 / 39.08	1.50 / 35.73	1.08 / 33.70	1.32 / 34.09
	3 \times	2.28 / 35.82	1.21 / 32.28	0.86 / 30.65	0.74 / 29.98
	4 \times	2.06 / 33.67	1.12 / 30.44	0.87 / 29.15	0.52 / 27.84
EDSR +Ours	2 \times	2.86 / 41.92	2.04 / 37.43	2.25 / 35.86	2.03 / 36.17
	3 \times	2.43 / 38.27	1.55 / 33.93	1.83 / 32.67	1.31 / 31.81
	4 \times	1.98 / 35.87	1.03 / 31.93	1.49 / 30.95	0.78 / 29.33
CARN	2 \times	2.58 / 38.56	1.54 / 35.28	1.19 / 33.47	1.14 / 32.96
	3 \times	2.25 / 35.24	1.28 / 31.94	0.99 / 30.45	0.70 / 29.28
	4 \times	2.02 / 33.23	1.13 / 30.17	0.91 / 29.01	0.44 / 27.35
CARN +Ours	2 \times	2.80 / 41.67	1.98 / 36.99	2.29 / 35.70	2.07 / 35.35
	3 \times	2.28 / 37.92	1.40 / 33.62	1.80 / 32.46	1.34 / 31.19
	4 \times	2.07 / 35.80	1.17 / 31.89	1.60 / 30.97	0.99 / 29.11

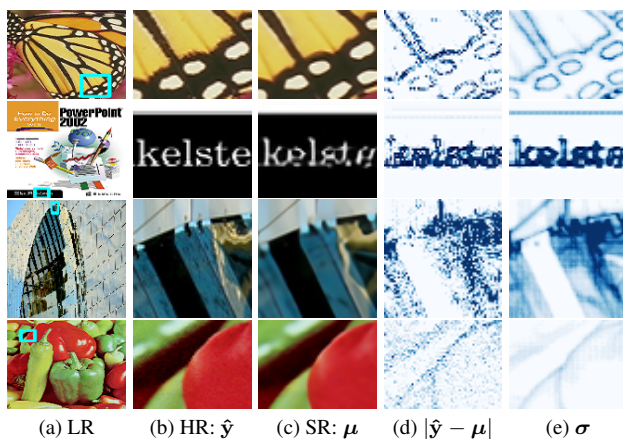


Figure 7. The last column (7e) visualizes the estimated uncertainty σ in 3 \times SR. Dark color indicates large variance, *i.e.*, high uncertainty. Considering the visual differences between HR and SR images and rael residual error (7d), σ depicts a promising uncertainty estimation that approximates the error with high fidelity.

with EDSR [47] and CARN [2] in Table 7. The original EDSR/CARN networks fail to consider the model uncertainty, hence we use their average fitting error $\mathbb{E}_{\mathcal{D}}[|\hat{y} - \mu|]$ calculated on the training dataset \mathcal{D} to create a constant uncertainty estimation, which corresponds to baseline results in Table 7. Any improvement over the baseline reflects a sensible estimate of uncertainty. It is shown that PLL for high upscaling factors are generally low, which indicates that reconstructed 4 \times image itself can be unreliable, *i.e.*, networks fail to recognize the hidden mistakes.

To improve the interpretability of the model uncertainty, we visualize the predicted σ in Figure 7e. It is shown that the estimated uncertainty strongly correlates with the actual residual error $|\hat{y} - \mu|$. We also report the PSNR results between them to further evaluate the uncertainty quality fairly since PLL has been criticized for being vulnerable to outliers [62].

5. Conclusions

In this paper, we present a novel learning process for single image super-resolution with neural networks. Instead of best fitting the ground-truth HR images, we introduce a posterior distribution $P(y|x; \mathbf{W})$ of underlying natural images y . By sampling from $P(y|x; \mathbf{W})$, the learning process serves as a multiple-valued mapping that better approximates the local manifold corresponding to the observed HR image. The experiments show that our method can produce SR images with minimal artifacts and the predicted standard deviation of $P(y|x; \mathbf{W})$, as a by-product, allows us to make meaningful estimations on the model uncertainty.

References

- [1] Eirikur Agustsson and Radu Timofte. Ntire 2017 challenge on single image super-resolution: Dataset and study. In *The IEEE Conference on Computer Vision and Pattern Recognition (CVPR) Workshops*, July 2017. 5, 6

- [2] Namhyuk Ahn, Byungkon Kang, and Kyung-Ah Sohn. Fast, accurate, and lightweight super-resolution with cascading residual network. In Vittorio Ferrari, Martial Hebert, Cristian Sminchisescu, and Yair Weiss, editors, *Computer Vision - ECCV 2018 - 15th European Conference, Munich, Germany, September 8-14, 2018, Proceedings, Part X*, volume 11214 of *Lecture Notes in Computer Science*, pages 256–272. Springer, 2018. 5, 6, 7, 8
- [3] Jan P. Allebach and Ping Wah Wong. Edge-directed interpolation. In *Proceedings 1996 International Conference on Image Processing, Lausanne, Switzerland, September 16-19, 1996*, pages 707–710. IEEE Computer Society, 1996. 2
- [4] Joshua Batson and Loïc Royer. Noise2self: Blind denoising by self-supervision. In Kamalika Chaudhuri and Ruslan Salakhutdinov, editors, *Proceedings of the 36th International Conference on Machine Learning, ICML 2019, 9-15 June 2019, Long Beach, California, USA*, volume 97 of *Proceedings of Machine Learning Research*, pages 524–533. PMLR, 2019. 2
- [5] Marco Bevilacqua, Aline Roumy, Christine Guillemot, and Marie-Line Alberi-Morel. Low-complexity single-image super-resolution based on nonnegative neighbor embedding. In Richard Bowden, John P. Collomosse, and Krystian Mikolajczyk, editors, *British Machine Vision Conference, BMVC 2012, Surrey, UK, September 3-7, 2012*, pages 1–10. BMVA Press, 2012. 2
- [6] Marco Bevilacqua, Aline Roumy, Christine Guillemot, and Marie-Line Alberi-Morel. Low-complexity single-image super-resolution based on nonnegative neighbor embedding. In Richard Bowden, John P. Collomosse, and Krystian Mikolajczyk, editors, *British Machine Vision Conference, BMVC 2012, Surrey, UK, September 3-7, 2012*, pages 1–10. BMVA Press, 2012. 5, 6, 7, 8
- [7] Joan Bruna, Pablo Sprechmann, and Yann LeCun. Super-resolution with deep convolutional sufficient statistics. In Yoshua Bengio and Yann LeCun, editors, *4th International Conference on Learning Representations, ICLR 2016, San Juan, Puerto Rico, May 2-4, 2016, Conference Track Proceedings*, 2016. 2, 3
- [8] Antoni Buades, Bartomeu Coll, and Jean-Michel Morel. A non-local algorithm for image denoising. In *2005 IEEE Computer Society Conference on Computer Vision and Pattern Recognition (CVPR 2005), 20-26 June 2005, San Diego, CA, USA*, pages 60–65. IEEE Computer Society, 2005. 3
- [9] Antoni Buades, Bartomeu Coll, and Jean-Michel Morel. A review of image denoising algorithms, with a new one. *Multiscale Model. Simul.*, 4(2):490–530, 2005. 3
- [10] Thang D. Bui, Daniel Hernández-Lobato, José Miguel Hernández-Lobato, Yingzhen Li, and Richard E. Turner. Deep gaussian processes for regression using approximate expectation propagation. In Maria-Florina Balcan and Kilian Q. Weinberger, editors, *Proceedings of the 33rd International Conference on Machine Learning, ICML 2016, New York City, NY, USA, June 19-24, 2016*, volume 48 of *JMLR Workshop and Conference Proceedings*, pages 1472–1481. JMLR.org, 2016. 7
- [11] Jose Caballero, Christian Ledig, Andrew P. Aitken, Alejandro Acosta, Johannes Totz, Zehan Wang, and Wenzhe Shi. Real-time video super-resolution with spatio-temporal networks and motion compensation. In *2017 IEEE Conference on Computer Vision and Pattern Recognition, CVPR 2017, Honolulu, HI, USA, July 21-26, 2017*, pages 2848–2857. IEEE Computer Society, 2017. 1
- [12] Jianrui Cai, Hui Zeng, Hongwei Yong, Zisheng Cao, and Lei Zhang. Toward real-world single image super-resolution: A new benchmark and a new model. In *2019 IEEE/CVF International Conference on Computer Vision, ICCV 2019, Seoul, Korea (South), October 27 - November 2, 2019*, pages 3086–3095. IEEE, 2019. 5, 6
- [13] Hong Chang, Dit-Yan Yeung, and Yimin Xiong. Super-resolution through neighbor embedding. In *2004 IEEE Computer Society Conference on Computer Vision and Pattern Recognition (CVPR 2004), with CD-ROM, 27 June - 2 July 2004, Washington, DC, USA*, pages 275–282. IEEE Computer Society, 2004. 2
- [14] Hanting Chen, Yunhe Wang, Tianyu Guo, Chang Xu, Yiping Deng, Zhenhua Liu, Siwei Ma, Chunjing Xu, Chao Xu, and Wen Gao. Pre-trained image processing transformer. *CoRR*, abs/2012.00364, 2020. 2
- [15] Yuhua Chen, Feng Shi, Anthony G. Christodoulou, Yibin Xie, Zhengwei Zhou, and Debiao Li. Efficient and accurate MRI super-resolution using a generative adversarial network and 3d multi-level densely connected network. In Alejandro F. Frangi, Julia A. Schnabel, Christos Davatzikos, Carlos Alberola-López, and Gabor Fichtinger, editors, *Medical Image Computing and Computer Assisted Intervention - MICCAI 2018 - 21st International Conference, Granada, Spain, September 16-20, 2018, Proceedings, Part I*, volume 11070 of *Lecture Notes in Computer Science*, pages 91–99. Springer, 2018. 2
- [16] Guoan Cheng, Ai Matsune, Qiuyu Li, Leilei Zhu, Huaijuan Zang, and Shu Zhan. Encoder-decoder residual network for real super-resolution. In *IEEE Conference on Computer Vision and Pattern Recognition Workshops, CVPR Workshops 2019, Long Beach, CA, USA, June 16-20, 2019*, pages 2169–2178. Computer Vision Foundation / IEEE, 2019. 2
- [17] Tao Dai, Jianrui Cai, Yongbing Zhang, Shu-Tao Xia, and Lei Zhang. Second-order attention network for single image super-resolution. In *IEEE Conference on Computer Vision and Pattern Recognition, CVPR 2019, Long Beach, CA, USA, June 16-20, 2019*, pages 11065–11074. Computer Vision Foundation / IEEE, 2019. 1, 2, 5, 7
- [18] Emily L. Denton, Soumith Chintala, Arthur Szlam, and Rob Fergus. Deep generative image models using a laplacian pyramid of adversarial networks. In Corinna Cortes, Neil D. Lawrence, Daniel D. Lee, Masashi Sugiyama, and Roman Garnett, editors, *Advances in Neural Information Processing Systems 28: Annual Conference on Neural Information Processing Systems 2015, December 7-12, 2015, Montreal, Quebec, Canada*, pages 1486–1494, 2015. 2
- [19] Carl Doersch. Tutorial on variational autoencoders. *CoRR*, abs/1606.05908, 2016. 3, 4
- [20] Chao Dong, Chen Change Loy, Kaiming He, and Xiaoou Tang. Learning a deep convolutional network for image super-resolution. In David J. Fleet, Tomás Pajdla, Bernt Schiele, and Tinne Tuytelaars, editors, *Computer Vision -*

- ECCV 2014 - 13th European Conference, Zurich, Switzerland, September 6-12, 2014, Proceedings, Part IV*, volume 8692 of *Lecture Notes in Computer Science*, pages 184–199. Springer, 2014. 1, 2
- [21] Chao Dong, Chen Change Loy, and Xiaoou Tang. Accelerating the super-resolution convolutional neural network. In Bastian Leibe, Jiri Matas, Nicu Sebe, and Max Welling, editors, *Computer Vision - ECCV 2016 - 14th European Conference, Amsterdam, The Netherlands, October 11-14, 2016, Proceedings, Part II*, volume 9906 of *Lecture Notes in Computer Science*, pages 391–407. Springer, 2016. 1, 2, 5
- [22] Weisheng Dong, Guangming Shi, Yi Ma, and Xin Li. Image restoration via simultaneous sparse coding: Where structured sparsity meets gaussian scale mixture. *Int. J. Comput. Vis.*, 114(2-3):217–232, 2015. 2
- [23] Alexey Dosovitskiy and Thomas Brox. Generating images with perceptual similarity metrics based on deep networks. In Daniel D. Lee, Masashi Sugiyama, Ulrike von Luxburg, Isabelle Guyon, and Roman Garnett, editors, *Advances in Neural Information Processing Systems 29: Annual Conference on Neural Information Processing Systems 2016, December 5-10, 2016, Barcelona, Spain*, pages 658–666, 2016. 2
- [24] Gilad Freedman and Raanan Fattal. Image and video up-scaling from local self-examples. *ACM Trans. Graph.*, 30(2):12:1–12:11, 2011. 2
- [25] Yarín Gal and Zoubin Ghahramani. Dropout as a bayesian approximation: Representing model uncertainty in deep learning. In Maria-Florina Balcan and Kilian Q. Weinberger, editors, *Proceedings of the 33rd International Conference on Machine Learning, ICML 2016, New York City, NY, USA, June 19-24, 2016*, volume 48 of *JMLR Workshop and Conference Proceedings*, pages 1050–1059. JMLR.org, 2016. 2, 7
- [26] Qinquan Gao, Yan Zhao, Gen Li, and Tong Tong. Image super-resolution using knowledge distillation. In C. V. Jawahar, Hongdong Li, Greg Mori, and Konrad Schindler, editors, *Computer Vision - ACCV 2018 - 14th Asian Conference on Computer Vision, Perth, Australia, December 2-6, 2018, Revised Selected Papers, Part II*, volume 11362 of *Lecture Notes in Computer Science*, pages 527–541. Springer, 2018. 2
- [27] Xinbo Gao, Kaibing Zhang, Dacheng Tao, and Xuelong Li. Image super-resolution with sparse neighbor embedding. *IEEE Trans. Image Process.*, 21(7):3194–3205, 2012. 2
- [28] Zoubin Ghahramani. Probabilistic machine learning and artificial intelligence. *Nat.*, 521(7553):452–459, 2015. 2
- [29] Daniel Glasner, Shai Bagon, and Michal Irani. Super-resolution from a single image. In *IEEE 12th International Conference on Computer Vision, ICCV 2009, Kyoto, Japan, September 27 - October 4, 2009*, pages 349–356. IEEE Computer Society, 2009. 2
- [30] Xiangyu He, Zitao Mo, Peisong Wang, Yang Liu, Mingyuan Yang, and Jian Cheng. Ode-inspired network design for single image super-resolution. In *IEEE Conference on Computer Vision and Pattern Recognition, CVPR 2019, Long Beach, CA, USA, June 16-20, 2019*, pages 1732–1741. Computer Vision Foundation / IEEE, 2019. 2, 5, 6
- [31] José Miguel Hernández-Lobato and Ryan P. Adams. Probabilistic backpropagation for scalable learning of bayesian neural networks. In Francis R. Bach and David M. Blei, editors, *Proceedings of the 32nd International Conference on Machine Learning, ICML 2015, Lille, France, 6-11 July 2015*, volume 37 of *JMLR Workshop and Conference Proceedings*, pages 1861–1869. JMLR.org, 2015. 7
- [32] Jia-Bin Huang, Abhishek Singh, and Narendra Ahuja. Single image super-resolution from transformed self-exemplars. In *IEEE Conference on Computer Vision and Pattern Recognition, CVPR 2015, Boston, MA, USA, June 7-12, 2015*, pages 5197–5206. IEEE Computer Society, 2015. 5, 6, 7, 8
- [33] Zheng Hui, Xinbo Gao, Yunchu Yang, and Xiumei Wang. Lightweight image super-resolution with information multi-distillation network. In Laurent Amsaleg, Benoit Huet, Martha A. Larson, Guillaume Gravier, Hayley Hung, Chong-Wah Ngo, and Wei Tsang Ooi, editors, *Proceedings of the 27th ACM International Conference on Multimedia, MM 2019, Nice, France, October 21-25, 2019*, pages 2024–2032. ACM, 2019. 6
- [34] Zheng Hui, Xiumei Wang, and Xinbo Gao. Fast and accurate single image super-resolution via information distillation network. In *2018 IEEE Conference on Computer Vision and Pattern Recognition, CVPR 2018, Salt Lake City, UT, USA, June 18-22, 2018*, pages 723–731. IEEE Computer Society, 2018. 6
- [35] Sergey Ioffe and Christian Szegedy. Batch normalization: Accelerating deep network training by reducing internal covariate shift. In Francis R. Bach and David M. Blei, editors, *Proceedings of the 32nd International Conference on Machine Learning, ICML 2015, Lille, France, 6-11 July 2015*, volume 37 of *JMLR Workshop and Conference Proceedings*, pages 448–456. JMLR.org, 2015. 2
- [36] Justin Johnson, Alexandre Alahi, and Li Fei-Fei. Perceptual losses for real-time style transfer and super-resolution. In Bastian Leibe, Jiri Matas, Nicu Sebe, and Max Welling, editors, *Computer Vision - ECCV 2016 - 14th European Conference, Amsterdam, The Netherlands, October 11-14, 2016, Proceedings, Part II*, volume 9906 of *Lecture Notes in Computer Science*, pages 694–711. Springer, 2016. 2
- [37] Jiwon Kim, Jung Kwon Lee, and Kyoung Mu Lee. Accurate image super-resolution using very deep convolutional networks. In *2016 IEEE Conference on Computer Vision and Pattern Recognition, CVPR 2016, Las Vegas, NV, USA, June 27-30, 2016*, pages 1646–1654. IEEE Computer Society, 2016. 2, 6
- [38] Jiwon Kim, Jung Kwon Lee, and Kyoung Mu Lee. Deeply-recursive convolutional network for image super-resolution. In *2016 IEEE Conference on Computer Vision and Pattern Recognition, CVPR 2016, Las Vegas, NV, USA, June 27-30, 2016*, pages 1637–1645. IEEE Computer Society, 2016. 1, 2
- [39] Diederik P. Kingma and Jimmy Ba. Adam: A method for stochastic optimization. In Yoshua Bengio and Yann LeCun, editors, *3rd International Conference on Learning Representations, ICLR 2015, San Diego, CA, USA, May 7-9, 2015, Conference Track Proceedings*, 2015. 5
- [40] Diederik P. Kingma and Max Welling. Auto-encoding variational bayes. In Yoshua Bengio and Yann LeCun, editors,

- 2nd International Conference on Learning Representations, ICLR 2014, Banff, AB, Canada, April 14-16, 2014, Conference Track Proceedings, 2014. 3, 4
- [41] Christian Ledig, Lucas Theis, Ferenc Huszar, Jose Caballero, Andrew Cunningham, Alejandro Acosta, Andrew P. Aitken, Alykhan Tejani, Johannes Totz, Zehan Wang, and Wenzhe Shi. Photo-realistic single image super-resolution using a generative adversarial network. In *2017 IEEE Conference on Computer Vision and Pattern Recognition, CVPR 2017, Honolulu, HI, USA, July 21-26, 2017*, pages 105–114. IEEE Computer Society, 2017. 1, 2, 6, 8
- [42] Wonkyung Lee, Junghyup Lee, Dohyung Kim, and Bumsub Ham. Learning with privileged information for efficient image super-resolution. In Andrea Vedaldi, Horst Bischof, Thomas Brox, and Jan-Michael Frahm, editors, *Computer Vision - ECCV 2020 - 16th European Conference, Glasgow, UK, August 23-28, 2020, Proceedings, Part XXIV*, volume 12369 of *Lecture Notes in Computer Science*, pages 465–482. Springer, 2020. 2, 5, 6
- [43] Jaakko Lehtinen, Jacob Munkberg, Jon Hasselgren, Samuli Laine, Tero Karras, Miika Aittala, and Timo Aila. Noise2noise: Learning image restoration without clean data. In Jennifer G. Dy and Andreas Krause, editors, *Proceedings of the 35th International Conference on Machine Learning, ICML 2018, Stockholmsmässan, Stockholm, Sweden, July 10-15, 2018*, volume 80 of *Proceedings of Machine Learning Research*, pages 2971–2980. PMLR, 2018. 2, 4
- [44] Min Li and Truong Q. Nguyen. Markov random field model-based edge-directed image interpolation. *IEEE Trans. Image Process.*, 17(7):1121–1128, 2008. 2
- [45] Xin Li and Michael T. Orchard. New edge-directed interpolation. *IEEE Trans. Image Process.*, 10(10):1521–1527, 2001. 2
- [46] Jingyun Liang, Jiezhong Cao, Guolei Sun, Kai Zhang, Luc Van Gool, and Radu Timofte. Swinir: Image restoration using swin transformer. *CoRR*, abs/2108.10257, 2021. 2
- [47] Bee Lim, Sanghyun Son, Heewon Kim, Seungjun Nah, and Kyoung Mu Lee. Enhanced deep residual networks for single image super-resolution. In *2017 IEEE Conference on Computer Vision and Pattern Recognition Workshops, CVPR Workshops 2017, Honolulu, HI, USA, July 21-26, 2017*, pages 1132–1140. IEEE Computer Society, 2017. 1, 2, 5, 6, 7, 8
- [48] Jie Liu, Wenjie Zhang, Yuting Tang, Jie Tang, and Gangshan Wu. Residual feature aggregation network for image super-resolution. In *2020 IEEE/CVF Conference on Computer Vision and Pattern Recognition, CVPR 2020, Seattle, WA, USA, June 13-19, 2020*, pages 2356–2365. IEEE, 2020. 1
- [49] Pengju Liu, Hongzhi Zhang, Kai Zhang, Liang Lin, and Wangmeng Zuo. Multi-level wavelet-cnn for image restoration. In *2018 IEEE Conference on Computer Vision and Pattern Recognition Workshops, CVPR Workshops 2018, Salt Lake City, UT, USA, June 18-22, 2018*, pages 773–782. IEEE Computer Society, 2018. 2
- [50] Xiao-Jiao Mao, Chunhua Shen, and Yu-Bin Yang. Image restoration using very deep convolutional encoder-decoder networks with symmetric skip connections. In Daniel D. Lee, Masashi Sugiyama, Ulrike von Luxburg, Isabelle Guyon, and Roman Garnett, editors, *Advances in Neural Information Processing Systems 29: Annual Conference on Neural Information Processing Systems 2016, December 5-10, 2016, Barcelona, Spain*, pages 2802–2810, 2016. 2
- [51] David R. Martin, Charless C. Fowlkes, Doron Tal, and Jitendra Malik. A database of human segmented natural images and its application to evaluating segmentation algorithms and measuring ecological statistics. In *Proceedings of the Eighth International Conference On Computer Vision (ICCV-01), Vancouver, British Columbia, Canada, July 7-14, 2001 - Volume 2*, pages 416–425. IEEE Computer Society, 2001. 5, 6, 7, 8
- [52] Michaël Mathieu, Camille Couprie, and Yann LeCun. Deep multi-scale video prediction beyond mean square error. In Yoshua Bengio and Yann LeCun, editors, *4th International Conference on Learning Representations, ICLR 2016, San Juan, Puerto Rico, May 2-4, 2016, Conference Track Proceedings*, 2016. 2
- [53] Yusuke Matsui, Kota Ito, Yuji Aramaki, Azuma Fujimoto, Toru Ogawa, Toshihiko Yamasaki, and Kiyoharu Aizawa. Sketch-based manga retrieval using manga109 dataset. *Multim. Tools Appl.*, 76(20):21811–21838, 2017. 5, 7
- [54] Yiqun Mei, Yuchen Fan, and Yuqian Zhou. Image super-resolution with non-local sparse attention. In *IEEE Conference on Computer Vision and Pattern Recognition, CVPR 2021, virtual, June 19-25, 2021*, pages 3517–3526. Computer Vision Foundation / IEEE, 2021. 2, 7
- [55] Yiqun Mei, Yuchen Fan, Yuqian Zhou, Lichao Huang, Thomas S. Huang, and Honghui Shi. Image super-resolution with cross-scale non-local attention and exhaustive self-exemplars mining. In *2020 IEEE/CVF Conference on Computer Vision and Pattern Recognition, CVPR 2020, Seattle, WA, USA, June 13-19, 2020*, pages 5689–5698. IEEE, 2020. 1, 2
- [56] John W. Miller, Rodney M. Goodman, and Padhraic Smyth. On loss functions which minimize to conditional expected values and posterior probabilities. *IEEE Trans. Inf. Theory*, 39(4):1404–1408, 1993. 1
- [57] Jing Mu, Xinfeng Zhang, Shuyuan Zhu, and Ruiqin Xiong. Riemannian loss for image restoration. In *IEEE Conference on Computer Vision and Pattern Recognition Workshops, CVPR Workshops 2019, Long Beach, CA, USA, June 16-20, 2019*, pages 502–504. Computer Vision Foundation / IEEE, 2019. 6
- [58] Ben Niu, Weilei Wen, Wenqi Ren, Xiangde Zhang, Lianping Yang, Shuzhen Wang, Kaihao Zhang, Xiaochun Cao, and Haifeng Shen. Single image super-resolution via a holistic attention network. In Andrea Vedaldi, Horst Bischof, Thomas Brox, and Jan-Michael Frahm, editors, *Computer Vision - ECCV 2020 - 16th European Conference, Glasgow, UK, August 23-28, 2020, Proceedings, Part XII*, volume 12357 of *Lecture Notes in Computer Science*, pages 191–207. Springer, 2020. 1, 2, 5, 7
- [59] Adam Paszke, Sam Gross, Francisco Massa, Adam Lerer, James Bradbury, Gregory Chanan, Trevor Killeen, Zeming Lin, Natalia Gimelshein, Luca Antiga, Alban Desmaison,

- Andreas Köpf, Edward Yang, Zachary DeVito, Martin Raison, Alykhan Tejani, Sasank Chilamkurthy, Benoit Steiner, Lu Fang, Junjie Bai, and Soumith Chintala. Pytorch: An imperative style, high-performance deep learning library. In Hanna M. Wallach, Hugo Larochelle, Alina Beygelzimer, Florence d’Alché-Buc, Emily B. Fox, and Roman Garnett, editors, *Advances in Neural Information Processing Systems 32: Annual Conference on Neural Information Processing Systems 2019, NeurIPS 2019, December 8-14, 2019, Vancouver, BC, Canada*, pages 8024–8035, 2019. [5](#)
- [60] Yuhui Quan, Mingqin Chen, Tongyao Pang, and Hui Ji. Self2self with dropout: Learning self-supervised denoising from single image. In *2020 IEEE/CVF Conference on Computer Vision and Pattern Recognition, CVPR 2020, Seattle, WA, USA, June 13-19, 2020*, pages 1887–1895. Computer Vision Foundation / IEEE, 2020. [2](#)
- [61] George Seif and Dimitrios Androutsos. Edge-based loss function for single image super-resolution. In *2018 IEEE International Conference on Acoustics, Speech and Signal Processing, ICASSP 2018, Calgary, AB, Canada, April 15-20, 2018*, pages 1468–1472. IEEE, 2018. [6](#)
- [62] Reinhard Selten. Axiomatic characterization of the quadratic scoring rule. *Experimental Economics*, 1(1):43–61, 1998. [8](#)
- [63] Daniel W Strock. *Probability theory: an analytic view*. Cambridge university press, 2010. [1](#)
- [64] Jian Sun, Zongben Xu, and Heung-Yeung Shum. Image super-resolution using gradient profile prior. In *2008 IEEE Computer Society Conference on Computer Vision and Pattern Recognition (CVPR 2008), 24-26 June 2008, Anchorage, Alaska, USA*. IEEE Computer Society, 2008. [2](#)
- [65] Yu-Wing Tai, Shuaicheng Liu, Michael S. Brown, and Stephen Lin. Super resolution using edge prior and single image detail synthesis. In *The Twenty-Third IEEE Conference on Computer Vision and Pattern Recognition, CVPR 2010, San Francisco, CA, USA, 13-18 June 2010*, pages 2400–2407. IEEE Computer Society, 2010. [2](#)
- [66] Ying Tai, Jian Yang, and Xiaoming Liu. Image super-resolution via deep recursive residual network. In *2017 IEEE Conference on Computer Vision and Pattern Recognition, CVPR 2017, Honolulu, HI, USA, July 21-26, 2017*, pages 2790–2798. IEEE Computer Society, 2017. [1](#)
- [67] Mattias Teye, Hossein Azizpour, and Kevin Smith. Bayesian uncertainty estimation for batch normalized deep networks. In Jennifer G. Dy and Andreas Krause, editors, *Proceedings of the 35th International Conference on Machine Learning, ICML 2018, Stockholm, Sweden, July 10-15, 2018*, volume 80 of *Proceedings of Machine Learning Research*, pages 4914–4923. PMLR, 2018. [2](#), [7](#)
- [68] Radu Timofte, Vincent De Smet, and Luc Van Gool. A+ adjusted anchored neighborhood regression for fast super-resolution. In Daniel Cremers, Ian D. Reid, Hideo Saito, and Ming-Hsuan Yang, editors, *Computer Vision - ACCV 2014 - 12th Asian Conference on Computer Vision, Singapore, Singapore, November 1-5, 2014, Revised Selected Papers, Part IV*, volume 9006 of *Lecture Notes in Computer Science*, pages 111–126. Springer, 2014. [2](#), [5](#)
- [69] Tong Tong, Gen Li, Xiejie Liu, and Qinquan Gao. Image super-resolution using dense skip connections. In *International Conference on Computer Vision, ICCV 2017, Venice, Italy, October 22-29, 2017*, pages 4809–4817. IEEE Computer Society, 2017. [2](#)
- [70] Dmitry Ulyanov, Andrea Vedaldi, and Victor S. Lempitsky. Deep image prior. In *2018 IEEE Conference on Computer Vision and Pattern Recognition, CVPR 2018, Salt Lake City, UT, USA, June 18-22, 2018*, pages 9446–9454. IEEE Computer Society, 2018. [2](#)
- [71] Zhangyang Wang, Yingzhen Yang, Zhaowen Wang, Shiyu Chang, Jianchao Yang, and Thomas S. Huang. Learning super-resolution jointly from external and internal examples. *IEEE Trans. Image Process.*, 24(11):4359–4371, 2015. [2](#)
- [72] Chih-Yuan Yang and Ming-Hsuan Yang. Fast direct super-resolution by simple functions. In *IEEE International Conference on Computer Vision, ICCV 2013, Sydney, Australia, December 1-8, 2013*, pages 561–568. IEEE Computer Society, 2013. [2](#)
- [73] Fuzhi Yang, Huan Yang, Jianlong Fu, Hongtao Lu, and Baining Guo. Learning texture transformer network for image super-resolution. In *2020 IEEE/CVF Conference on Computer Vision and Pattern Recognition, CVPR 2020, Seattle, WA, USA, June 13-19, 2020*, pages 5790–5799. Computer Vision Foundation / IEEE, 2020. [2](#)
- [74] Jianchao Yang, John Wright, Thomas S. Huang, and Yi Ma. Image super-resolution via sparse representation. *IEEE Trans. Image Process.*, 19(11):2861–2873, 2010. [2](#)
- [75] Xin Yu and Fatih Porikli. Ultra-resolving face images by discriminative generative networks. In Bastian Leibe, Jiri Matas, Nicu Sebe, and Max Welling, editors, *Computer Vision - ECCV 2016 - 14th European Conference, Amsterdam, The Netherlands, October 11-14, 2016, Proceedings, Part V*, volume 9909 of *Lecture Notes in Computer Science*, pages 318–333. Springer, 2016. [2](#)
- [76] Linwei Yue, Huanfeng Shen, Jie Li, Qiangqiang Yuan, Hongyan Zhang, and Liangpei Zhang. Image super-resolution: The techniques, applications, and future. *Signal Process.*, 128:389–408, 2016. [2](#)
- [77] Roman Zeyde, Michael Elad, and Matan Protter. On single image scale-up using sparse-representations. In Jean-Daniel Boissonnat, Patrick Chenin, Albert Cohen, Christian Gout, Tom Lyche, Marie-Laurence Mazure, and Larry L. Schumaker, editors, *Curves and Surfaces - 7th International Conference, Avignon, France, June 24-30, 2010, Revised Selected Papers*, volume 6920 of *Lecture Notes in Computer Science*, pages 711–730. Springer, 2010. [5](#), [6](#), [7](#), [8](#)
- [78] Lei Zhang and Xiaolin Wu. An edge-guided image interpolation algorithm via directional filtering and data fusion. *IEEE Trans. Image Process.*, 15(8):2226–2238, 2006. [2](#)
- [79] Yulun Zhang, Kunpeng Li, Kai Li, Lichen Wang, Bineng Zhong, and Yun Fu. Image super-resolution using very deep residual channel attention networks. In Vittorio Ferrari, Martial Hebert, Cristian Sminchisescu, and Yair Weiss, editors, *Computer Vision - ECCV 2018 - 15th European Conference, Munich, Germany, September 8-14, 2018, Proceedings, Part VII*, volume 11211 of *Lecture Notes in Computer Science*, pages 294–310. Springer, 2018. [1](#), [2](#), [6](#), [7](#), [8](#)
- [80] Yulun Zhang, Yapeng Tian, Yu Kong, Bineng Zhong, and Yun Fu. Residual dense network for image super-resolution.

In *2018 IEEE Conference on Computer Vision and Pattern Recognition, CVPR 2018, Salt Lake City, UT, USA, June 18-22, 2018*, pages 2472–2481. IEEE Computer Society, 2018. [2](#)

- [81] Hang Zhao, Orazio Gallo, Iuri Frosio, and Jan Kautz. Loss functions for image restoration with neural networks. *IEEE Trans. Computational Imaging*, 3(1):47–57, 2017. [1](#)
- [82] Shangchen Zhou, Jiawei Zhang, Wangmeng Zuo, and Chen Change Loy. Cross-scale internal graph neural network for image super-resolution. In Hugo Larochelle, Marc’Aurelio Ranzato, Raia Hadsell, Maria-Florina Balcan, and Hsuan-Tien Lin, editors, *Advances in Neural Information Processing Systems 33: Annual Conference on Neural Information Processing Systems 2020, NeurIPS 2020, December 6-12, 2020, virtual*, 2020. [1](#), [2](#), [5](#)